Computational Mechanics (2020) 65:587–595
https://doi.org/10.1007/s00466-019-01784-2

ORIGINAL PAPER

Viscoelasticity of the axon limits stretch-mediated growth

Lucy M. Wang[1] · **Ellen Kuhl**[1]

Received: 27 May 2019 / Accepted: 4 October 2019 / Published online: 28 October 2019

Abstract
Understanding how axons fail is critical to preventing brain injury. From stretch experiments, we know how axons respond to forces on the time scales of milliseconds and days. Yet, there is no mechanical model that explains the behavior of the axon at both short and long time scales. Here we propose a constitutive model to study the limits of stretch-mediated axonal disconnection at different time scales. Our model combines viscoelasticity using a neo-Hookean standard linear solid and growth using stress-mediated accelerated elongation. By limiting peak and average membrane tensions, our model predicts critical elongations and elongation rates. Interestingly, the critical elongation rate is not constant, but increases after an acclimation period. Combining viscoelasticity and growth is essential to simulate axonal disconnection in stretch-mediated growth at both short and long time scales. Our model can help optimize axonal stretch experiments and provides insight into the interacting time scales within the axon.

Keywords Tension · Viscosity · Growth · Axon

1 Introduction

In the neuron, multiple slender processes extend from the cell body to form connections with other cells. The longest of these is known as the axon. Axons grow to lengths of over 1 m long in humans and over 10 m long in the blue whale [30]. It is estimated that in order to reach these lengths, rates of axonal growth can be as high as 2 cm/day [6]. How the axon achieves this growth rate remains unsettled.

Earlier studies on axonal growth focused on the first phase during which chemical and physical cues guide the axon to its target [24,25]. Interest then turned to growth that occurs after the axon has reached its target and formed a connection [3,34,40]. It is thought that during this phase, organ growth triggers axon growth as the distance between the end target and the soma increases [18]. This is illustrated in Fig. 1. Studies have replicated this phenomenon in vitro by using microneedles to pull on individual axons [40] and by using micro stepper motors to apply incremental displacements to neuron populations [34]. In the experiments using the micro stepper motor, axons were elongated using short displacement increments followed by periods of relaxation. The overall elongation rate could be adjusted either by increasing the magnitude of the displacement increments or by adjusting the duration of the relaxation period. If elongation was applied slowly enough, growth was observed. On the other hand, if the elongation was too rapid, growth could not keep up, and disconnection occurred. While low levels of stretch promoted growth, higher levels led to axonal injury and disconnection [31,34].

Understanding the threshold between disconnection and growth has potential applications both in limb lengthening procedures and in nerve repair. In limb lengthening, nerves must grow along with the rest of the surrounding tissues [1]. Elongating the limb at too high a rate can lead to impaired nerve function [33]. The disconnection threshold influences the maximum growth rate achievable during the limb lengthening procedure. In nerve repair, gradual lengthening has been explored as an alternative to grafting, which is currently the gold standard [38]. Grafts are preferred in repairing large nerve gaps, as a high level of tension is harmful for the regeneration process [20,35,36]. High levels of tension result when the two ends of the nerve are immediately pulled together and sutured. Taking advantage of axonal stretch growth, studies are exploring ways to elongate the nerve gradually prior to reconnection [38]. Gradual elongation has been attempted both intraoperatively [2,28] and via an implanted device [23,39]. The elongation time for

✉ Ellen Kuhl
ekuhl@stanford.edu

[1] Department of Mechanical Engineering, Stanford University, Stanford, CA 94305, USA

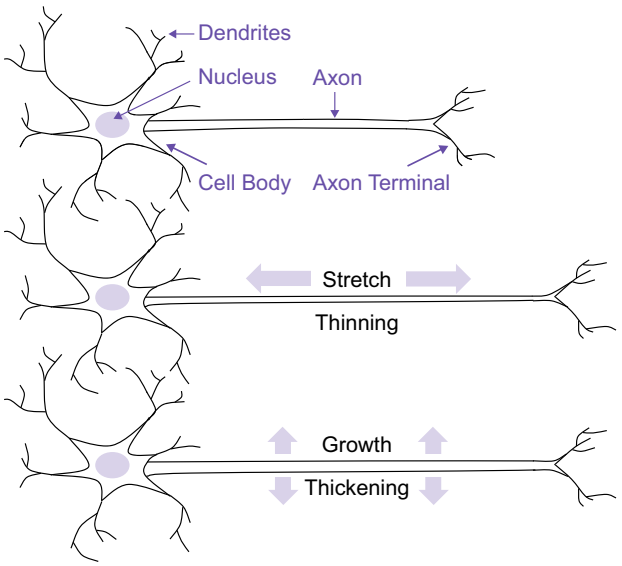

Fig. 1 Stretch-mediated axonal growth. A displacement is applied to the end of the axon. At first, this stretch is entirely viscoelastic, but over time, growth occurs. As the amount of growth increases, the viscoelastic part of the stretch decreases, leading to a decrease in stress. The presence of growth is often inferred from an increase in axon diameter

the intraoperative method ranges from minutes to an hour, whereas an implanted device can elongate over a period of 2 weeks [2,23,28,39]. Knowledge of the disconnection threshold would inform the selection of a repair method based on nerve gap size.

A computational model of axonal growth could be used to predict disconnection. Early phenomenological models of the axon represented its viscoelastic response at short time scales using the standard linear solid model [9] in which a dashpot added in series with the viscoelastic element represents growth [9,29]. More recently, three-dimensional continuum models incorporated growth using the multiplicative decomposition of the deformation gradient into elastic and inelastic parts [16,22]. In these studies, the elastic part is modeled as both hyperelastic [22] and viscoelastic [16], while the inelastic part represents growth. Other models have looked at smaller scales and calculated axonal growth rates based on the transport and action of cytoskeletal proteins [10,12,37]. These protein-level models can link membrane tension and protein production rates and provide insight into the stretch-limiting mechanisms. One such growth model, combined with a threshold on axon membrane tension, predicted disconnection thresholds that agreed well with experiments [32]. While the model explains disconnection behavior at long time scales, it does not explain the short time scale limits on displacement step magnitude and frequency.

Here, we propose a new model that integrates viscoelasticity and growth to predict axonal disconnection at both short and long time scales. Following the method used in previous studies, we multiplicatively decompose the deformation gradient into a viscoelastic and a growth part [16,22]. By applying thresholds on membrane tension, we show that the viscoelastic response of the axon governs disconnection at short time scales, whereas growth governs the behavior at long time scales.

2 Methods

2.1 Axonal growth

We represent axonal growth using a multiplicative decomposition of the deformation gradient $\mathbf{F}$,

$$\mathbf{F} = \mathbf{F}^{\mathrm{v}} \cdot \mathbf{F}^{\mathrm{g}} , \tag{1}$$

where $\mathbf{F}^{\mathrm{v}}$ is the viscoelastic part and $\mathbf{F}^{\mathrm{g}}$ is the growth part. We assume that the viscoelastic part is incompressible and that any change in cross-sectional area is solely due to the viscoelastic deformation. The total deformation gradient then becomes

$$\mathbf{F} = \lambda\, \mathbf{a}_0 \otimes \mathbf{a}_0 + 1/\sqrt{\lambda^{\mathrm{v}}}(\,\mathbf{I} - \mathbf{a}_0 \otimes \mathbf{a}_0\,) , \tag{2}$$

where λ and λ^{v} are the total and viscoelastic part of the stretch, $\mathbf{I}$ is the unit tensor, and $\mathbf{a}_0$ is the unit vector in the axon direction in the reference configuration. We model axonal growth as one-dimensional fiber growth and introduce the growth tensor as

$$\mathbf{F}^{\mathrm{g}} = \mathbf{I} + (\,\vartheta - 1\,)\, \mathbf{a}_0 \otimes \mathbf{a}_0 , \tag{3}$$

where ϑ is the growth multiplier that represents the increase in grown length [26,27]. In the following, we consider experiments of uniaxial axonal tension, for which the total stretch λ in the axonal direction $\mathbf{a}_0$ decomposes multiplicatively into a viscous part λ^{v} and a growth part λ^{g},

$$\lambda = \lambda^{\mathrm{v}}\, \lambda^{\mathrm{g}} \qquad \text{with} \qquad \lambda^{\mathrm{g}} = \vartheta . \tag{4}$$

We model the evolution of the growth multiplier as

$$\dot{\vartheta}(t) = f\,(t)\, \langle \sigma(t) - \sigma_{\mathrm{c}} \rangle , \tag{5}$$

where $f(t)$ represents a general function specifying how the strength of the growth trigger varies with time. σ is the normal Cauchy stress in the axonal direction, and σ_{c} is the stress threshold for growth to occur. The Macaulay bracket is defined as

$$\langle \sigma(t) - \sigma_{\mathrm{c}} \rangle = \begin{cases} 0 & \sigma \le \sigma_{\mathrm{c}} \\ \sigma(t) - \sigma_{\mathrm{c}} & \sigma > \sigma_{\mathrm{c}} \end{cases} . \tag{6}$$

Table 1 Parameters of the axon model

Parameter	Value	Unit	References
G_∞	10^{-9}	$\mathrm{Pa}^{-1}\,\mathrm{s}^{-1}$	[22]
G	10^{-7}	$\mathrm{Pa}^{-1}\,\mathrm{s}^{-1}$	[22]
τ_g	5.5e5	s	[22]
σ_c	0	Pa	[5]
γ_∞	2.05e−2	–	[9]
γ	9.795e−1	–	[9]
τ_v	100	s	[9]
μ	2.767e4	Pa	[9]
T_0	7.5e−4	$\mathrm{N\,m}^{-1}$	[32]

We choose the following form for $f(t)$,

$$f(t) = G_\infty - G\,\exp(-t/\tau_\mathrm{g})\,, \tag{7}$$

where G_∞, G, and τ_g are time constants of the growth model. We select this evolution law because it postulates that growth accelerates over time in agreement with experimental observations [31]. We calibrate the time constants G_∞, G, and τ_g in accordance with diameter recovery experiments [22] and select a stress threshold of $\sigma_\mathrm{c} = 0$ motivated by experimental observations [5].

2.2 Axonal viscosity

We calculate the normal Cauchy stress in the axonal direction using the viscoelastic part of the deformation gradient using a Prony series approach [4],

$$\sigma(t) = \int_{-\infty}^{t} g(t-s)\frac{\mathrm{d}}{\mathrm{d}s}\sigma_0(s)\,\mathrm{d}s\,. \tag{8}$$

Here $g(t)$ is the relaxation function for a standard linear solid,

$$g(t) = \gamma_\infty + \gamma\,\exp(-t/\tau_\mathrm{v})\,. \tag{9}$$

where γ_∞ is the long-term modulus of the relaxed axon, γ is the viscous relaxation coefficient, τ_v is the viscous relaxation time, and σ_0 is the initial stress [9]. We derive the initial axonal stress from the following stored-energy function for an incompressible neo-Hookean material [17],

$$\psi_0 = \frac{1}{2}\,\mu\,((\lambda^\mathrm{v})^2 + 2/\lambda^\mathrm{v} - 3)\,, \tag{10}$$

where μ is the shear modulus of the axon [9]. Table 1 summarizes the values of all the constitutive model parameters. The initial Cauchy stress becomes,

$$\sigma_0 = \lambda^\mathrm{v}\frac{\partial\psi_0}{\partial\lambda^\mathrm{v}} = \mu\,((\lambda^\mathrm{v})^2 - 1/\lambda^\mathrm{v})\,. \tag{11}$$

Now we define,

$$h(t) = \int_{-\infty}^{t} \exp(-(t-s)/\tau_\mathrm{v})\,\frac{\mathrm{d}}{\mathrm{d}s}\sigma_0(s)\,\mathrm{d}s\,, \tag{12}$$

so that the normal Cauchy stress in the axon direction simplifies to

$$\sigma(t) = \gamma_\infty\,\sigma_0(t) + \gamma\,h(t)\,. \tag{13}$$

2.3 Axonal disconnection

Following the literature [32], we assume that membrane tension governs axonal disconnection, and estimate the membrane tension from the stress output of our model. To do this, we assume a worst-case scenario in which the membrane carries all of the force on the axon,

$$T(t) = F(t)/C(t) + T_0 = \sigma(t)A(t)/C(t)\,, \tag{14}$$

where $F(t)$ is the force on the axon, $C(t)$ is the circumference, and $A(t)$ is the cross-sectional area. T_0 is the rest tension for which we used a value of $7.5\mathrm{e}{-4}\,\mathrm{N\,m}^{-1}$ [32]. Equation (14) simplifies to

$$T(t) = \frac{1}{4}\,\sigma(t)\,d(t) + T_0\,, \tag{15}$$

where $d(t)$ is the current axon diameter. Table 1 summarizes the parameter values of axonal growth, viscosity, and disconnection.

It has been observed in experiments that membrane strength is time dependent; lower tension levels can be sustained for longer periods, but higher tension levels can only be sustained for a few seconds [19]. We therefore introduce two levels of critical membrane tension. The higher threshold predicts disconnection if exceeded by the peak tension, which would be sustained for a few seconds, and the lower threshold predicts disconnection if exceeded by the time-averaged tension, which would be sustained for hours. To evaluate the ability of our model to predict axonal disconnection, we use displacement histories from elongation experiments as input to our model [31]. We then compare the resulting model predictions to the experimental observations.

2.4 Computational model

To solve the equations for axonal growth, viscosity, and disconnection for a given stretch history, $\lambda(t)$, we discretize the time interval of interest into discrete time steps and march forward incrementally in time. Since the evolution of the growth multiplier (7) depends nonlinearly on the growth multiplier itself, we perform a Newton Raphson iteration. To move forward from time t_n to time t_{n+1} at an increment $\Delta t = t_{n+1} - t_n$,

at the beginning of the time step, we initialize the growth multiplier ϑ_{n+1} and the stress σ_{n+1} with their known values from the previous time step and evaluate the time-discrete growth equation,

$$\vartheta_{n+1} = \vartheta_n + (\, G_\infty - G\, \exp(-t_{n+1}/\tau_g\,))\langle\, \sigma_n - \sigma_c\,\rangle \Delta t\,. \quad (16)$$

Using this result and the known prescribed total stretch, λ_{n+1}, we update the viscoelastic stretch,

$$\lambda^{\mathrm{v}}_{n+1} = \lambda_{n+1}/\vartheta_{n+1}\,, \quad (17)$$

the initial Cauchy stress,

$$\sigma_{0\,n+1} = \mu\,(\,(\lambda^{\mathrm{v}}_{n+1})^2 - 1/\lambda^{\mathrm{v}}_{n+1}\,)\,. \quad (18)$$

the value of h,

$$h_{n+1} = \exp(-\Delta t/\tau_{\mathrm{v}})h_n + \exp(-\Delta t/2\tau_{\mathrm{v}})(\sigma_{0\,n+1} - \sigma_{0\,n})\,, \quad (19)$$

and the Cauchy stress,

$$\sigma_{n+1} = \gamma_\infty\, \sigma_{0\,n+1} + \gamma\, h_{n+1}\,. \quad (20)$$

Finally, for the Newton Raphson iteration, we calculate the residual R,

$$\mathsf{R} = \vartheta_{n+1} - \vartheta_n - (G_\infty - G\exp(-t_{n+1}/\tau_g))(\sigma_{n+1} - \sigma_c)\Delta t, \quad (21)$$

and K, its linearization with respect to ϑ_{n+1},

$$\mathsf{K} = \frac{\mathrm{d}\mathsf{R}}{\mathrm{d}\vartheta_{n+1}} = 1 - (\,G_\infty - G\exp(-t_{n+1}/\tau_g)\,)\frac{\mathrm{d}\sigma_{n+1}}{\mathrm{d}\vartheta_{n+1}}\Delta t\,, \quad (22)$$

with

$$\frac{\mathrm{d}\sigma_{n+1}}{\mathrm{d}\vartheta_{n+1}} = -\mu\,(\gamma_\infty + \gamma\exp(-\Delta t/2\tau_{\mathrm{v}}))\,\frac{2\lambda^3_{\mathrm{v}\,n+1} + 1}{\lambda_{n+1}}\,. \quad (23)$$

We update the incremental growth multiplier,

$$\vartheta_{n+1} \leftarrow \vartheta_{n+1} - \mathsf{R}/\mathsf{K}\,, \quad (24)$$

and iterate until the residual R falls below a user-defined threshold. We then move to the next time step, and the iteration begins again.

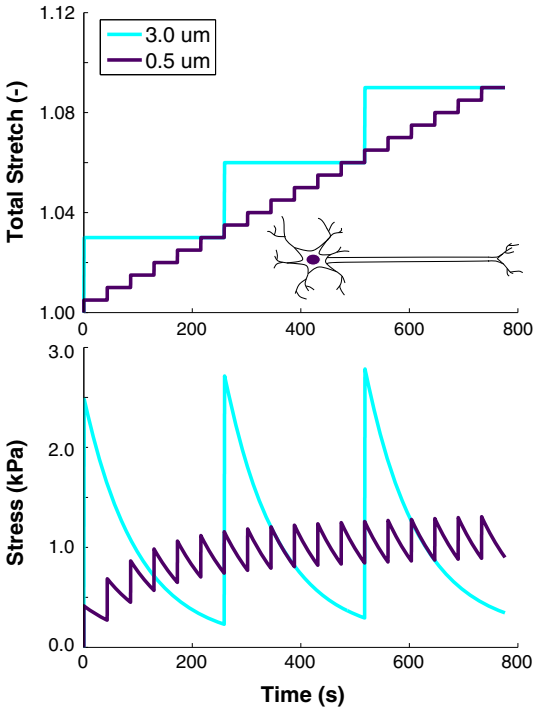

Fig. 2 Effects of displacement increment on stress. A net elongation rate of 1 mm/day can be achieved using different displacement increments, here 0.5 μm and 3.0 μm (top). At the same net elongation rate, the axon experiences different stresses depending on the step size (bottom). Larger displacement increments cause higher peak stresses

3 Results

3.1 Effects of displacement increment

In axon stretching experiments, a micro stepper motor is often used to control elongation [31]. A desired net elongation rate can be achieved using many small displacement steps or fewer larger steps. For an elastic material, the maximum stress simply depends on the overall displacement and is independent of the displacement increment. For a viscoelastic material, however, a larger displacement increment results in higher peak stresses.

Figure 2 displays the prescribed axonal stretch and the resulting stress for a 1 mm/day elongation rate using two different step sizes, 0.5 μm and 3.0 μm. While the mean stress is the same for both step sizes, the larger step size results in larger oscillations with respect to the mean. While Fig. 2 demonstrates the stress response over a short time period of 15 min, Fig. 3 illustrates the behavior over a longer time period of 1 day. At this longer time scale, the effects of growth become apparent. Initially, the average stress increases along with the increasing elongation. However, as time passes, growth occurs, and the average stress begins to decrease. Two modes of stress relaxation are observed in the model:

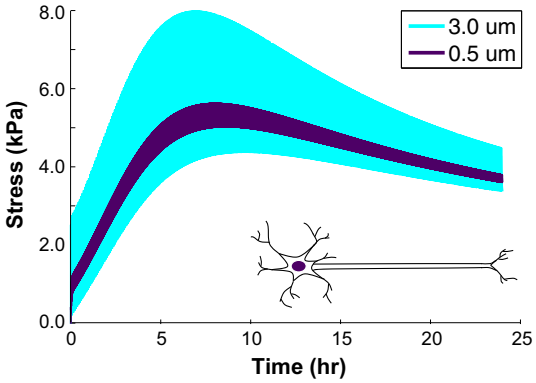

Fig. 3 Effects of displacement increment on average and peak stress. Over the course of a day, the average stress decreases as growth occurs. Larger displacement increments cause higher peak stresses, but do not affect the average stress

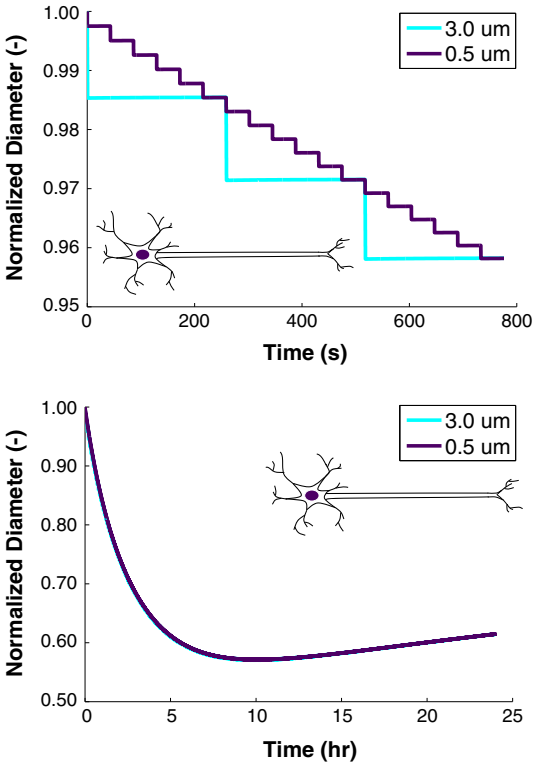

Fig. 4 Effects of displacement increment on axon diameter. On the short time scale, the axon diameter decreases with each applied displacement increment in accordance with the incompressibility assumption (top). On the long time scale, axon diameter decreases at first as applied elongation outpaces growth. As time progresses and growth increases, the diameter begins to recover (bottom)

Relaxation due to viscoelasticity occurs on a short time scale, and relaxation due to growth occurs on a longer time scale.

Figure 4 shows the effects of growth on the evolution of the axon diameter at short and long time scales. On short time scales (top), decreases in axon diameter closely follow the applied increase in axon length. On the long time scales

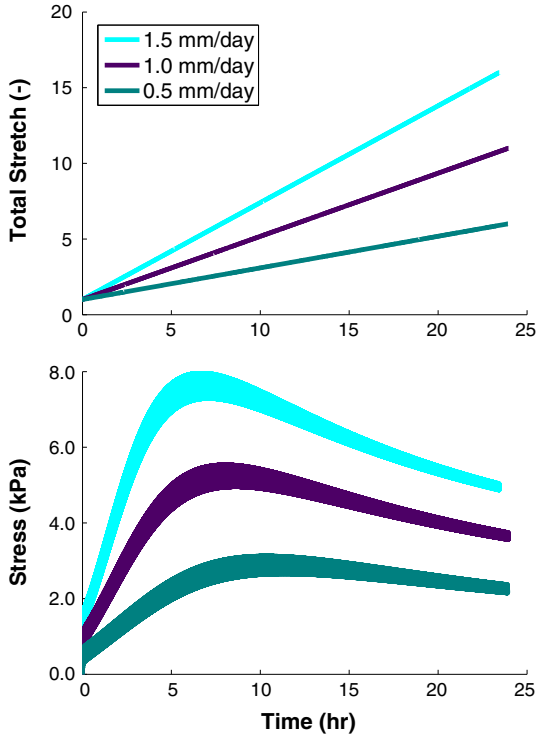

Fig. 5 Effects of net elongation rate. For a step size of 0.5 μm, the stretch rate can be adjusted by changing the length of the rest period between the displacements (top). Larger net elongation rates cause larger peak and average stresses (bottom)

(bottom), the axon diameter begins to recover as growth increases.

3.2 Effects of net elongation rate

For a given step size, we can achieve different net elongation rates by adjusting the length of the rest periods. Shortening the rest periods results in a faster elongation rate. Figure 5 illustrates that a shorter rest period gives the stress less time to decay, so increasing the elongation rate raises the average and peak stresses. We can see the effects of growth in the decay of the average stress over time: At faster elongation rates, the stress reaches higher magnitudes before decaying in response to growth. The magnitude of the asymptotic stress also increases with elongation rate.

3.3 Effects of accelerated stretch

To examine the ability of the axon to acclimate to increases in elongation rate, we apply a systematic accelerating elongation scheme. After the first 24 h, we increase the stretch rate from 1 to 2 mm/day. After days 3 and 5, we increase the rate again to 3 and 4 mm/day. Figure 6 illustrates the resulting stress response. Initially, the stress increases rapidly in response to the applied elongation. As growth occurs,

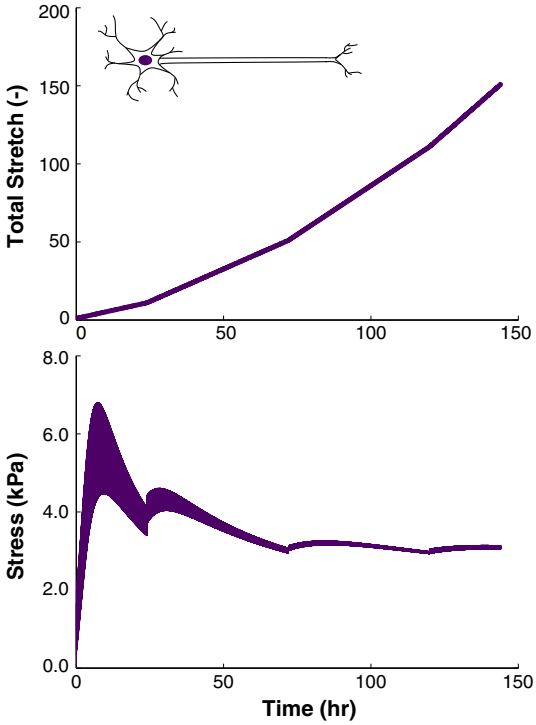

Fig. 6 Effects of accelerated stretch The elongation rate is increased gradually in increments of 1 mm/day after days 1, 3, and 5 over a period of 6 days (top). After an initial rapid increase, the stress decays as growth occurs (bottom)

the stress begins to decay. Every time the elongation rate increases, there is a corresponding peak in stress followed by a period of decay while the rate is held constant. Since the growth is accelerating over time, the stress remains relatively low despite the increasing elongation rate.

3.4 Predicting disconnection

Axonal stretch experiments show that for a 1 mm/day elongation rate, 2μm is the maximum step size that does not lead to disconnection. Furthermore, 1 mm/day is the maximum achievable elongation rate during the first 24 h for any step size. However, after the first day, the elongation rate can be increased without causing disconnection [31]. Comparing these observations to our model's estimates of the axon membrane tension, we deduce disconnection threshold values of 1.8 mN/m for average tension and 2.1 mN/m for peak tension.

Figure 7 highlights the disconnection thresholds for our two step sizes, 0.5 μm and 3 μm. Clearly, the lower threshold, the solid line, does not predict disconnection for either 0.5 μm or 3 μm since the average tension is the same for both and remains below the lower threshold. The higher threshold, the dashed line, predicts that the 3 μm step size would lead

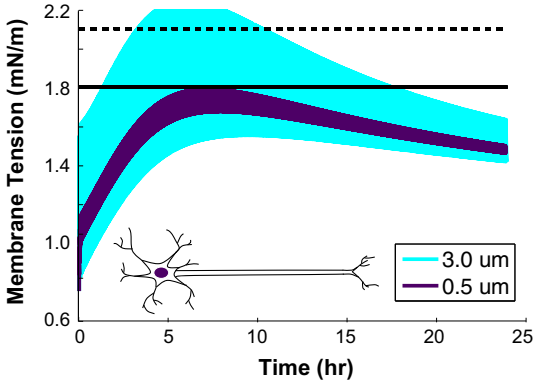

Fig. 7 Effects of displacement increment on disconnection. The lower disconnection threshold for the average membrane tension (solid line) does not predict disconnection for either displacement increment. The higher disconnection threshold for the peak membrane tension (dashed line) predicts that the 3 μm displacement increment will lead to disconnection

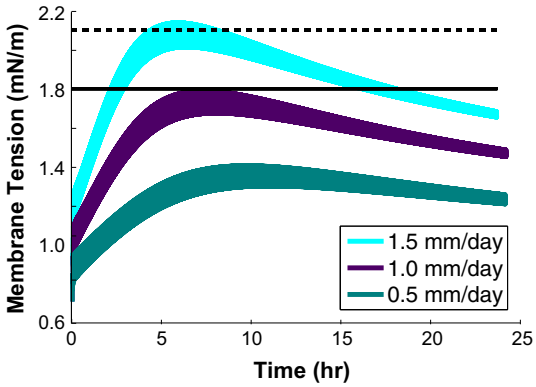

Fig. 8 Effects of net elongation rate on disconnection. The 1.5 mm/day elongation rate will lead to disconnection, since the membrane tension has exceeded both threshold for the average membrane tension (solid line) and for the peak membrane tension (dashed line). Smaller net elongation rates will not trigger disconnection

to disconnection, since the peak tension exceeds the higher threshold.

Figure 8 shows the disconnection thresholds for our three elongation rates, 0.5 mm/day, 1.0 mm/day, and 1.5 mm/day. The model predicts disconnection for the 1.5 mm/day elongation rate, but membrane tensions for the 1.0 mm/day and 0.5 mm/day rates remain below the disconnection thresholds. Finally, for the case of accelerated stretching, in Fig. 9, the accelerating growth rate keeps the tension values below the disconnection threshold, and the model predicts no disconnection.

3.5 Maximizing growth

To obtain the optimal stretch history for maximum growth, we fix the membrane tension at 1.8 mN/m, the threshold on average tension. We then solve for the stretch history

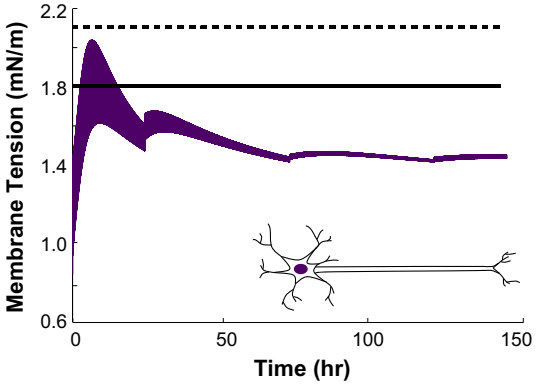

Fig. 9 Effects of accelerated stretch on disconnection. As elongation rate is increased, accelerated growth keeps the membrane tension below the disconnection thresholds for the average membrane tension (solid line) and for the peak membrane tension (dashed line)

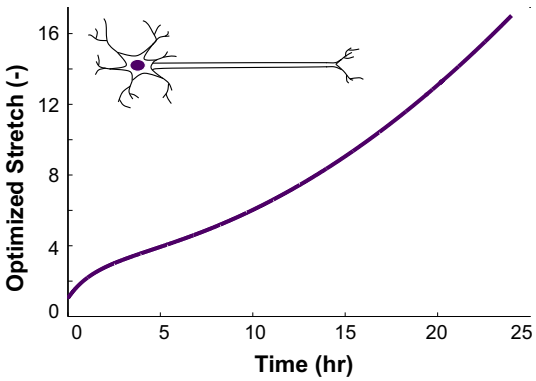

Fig. 10 Optimized stretch history. To maximize growth for a prescribed tension threshold, the optimal stretch history displays a characteristic S-shape form: initially, the stretch increases rapidly to maximize the trigger for growth. Then, the stretch rate decreases to prevent tension from exceeding the tension threshold. With increasing growth, the stretch rate can increase again

that will maintain this average tension. In this optimal case, we increase the stretch continuously instead of discretely in several steps. This minimizes the peak stresses and allows disconnection to be governed solely by the average tension. Figure 10 shows the optimal stretch history over the first day. The stretch increases rapidly at first to maximize the trigger for growth. The stretch rate must then decrease to prevent tension from surpassing the threshold. Finally, as growth increases, the stretch rate can be raised once again.

4 Discussion

Our model predicts a disconnection behavior that agrees with experimental observations [31]. At short time scales, our model explains that large displacement increments result in high peak membrane tensions, increasing the risk of axonal disconnection. For a given displacement step size, increasing the net elongation rate results in both higher average tensions and higher peak tensions. An excessively high elongation rate will naturally trigger disconnection. Interestingly, the accelerating growth evolution law allows increases in elongation rate since stresses decrease as growth occurs.

Pfister et al. [31] observed that during the first 24 h of elongation, the step size was limited to 2μm, and the net elongation rate could not exceed 1 mm/day. To agree with these values, our model requires a lower membrane tension threshold of 1.8 mN/m and a higher threshold of 2.1 mN/m. The lower threshold governs disconnection based on the time-averaged tension while the higher threshold governs disconnection based on the peak tension. These membrane tensions are slightly lower than the 5–12 mN/m range reported by Dai et al. for molluscan neurons [8]. This discrepancy could be caused by the time-dependent nature of the membrane strength. In red blood cells, Hategan et al. [19] observed that tensions of 4–7 mN/m led to rupture after only a few seconds. However, tensions as low as 1 mN/m could also cause rupture if sustained for a time period on the order of hours. Similarly, Evans et al. described the dependence of rupture tension on loading rate. Increasing the loading rate from 0.01 to 100 mN/m/s, they observed the rupture tension to increase from 2 to 30 mN/m [14]. In our model, the lower tension threshold of 1.8 mN/m governs the average tension, which is sustained for several hours. This threshold agrees with the observations of Hategan et al. [19]. The higher threshold of 2.1 mN/m is still in the lower range of the reported rupture tensions. This threshold governs the peak tension, which would only be sustained for a few seconds. Based on reported rupture tensions, a value of 2.1 mN/m would likely not cause disconnection after only a few seconds [14,19]. However, our 2.1 mN/m threshold could be describing a cumulative effect of short term excursions to higher tensions superposed on the baseline average tension.

In their model of axonal stretch growth, Purohit and Smith suggest a single threshold value of 1 mN/m to predict axonal disconnection [32]. Using this threshold, they can reproduce experimentally observed limits on net elongation rate. Their model can also predict the accommodation of higher elongation rates after an acclimation period. However, Purohit and Smith focus only on the effect of growth on membrane tension; they do not consider the effects of viscoelasticity. As a result, their model is limited in its predictive ability at short time scales and cannot prescribe limits on displacement step size. By incorporating viscoelasticity and a second tension threshold, we extend the model's predictive ability to both short and long time scales. As a result, we are able to predict limits on both displacement step size and elongation rate.

While our results suggest that our model can predict optimal displacement histories that avoid axonal disconnection, we used and estimated our parameter values from different studies and different cell types. Ideally, measurements should

be taken on the particular cell type of interest, so that parameters can be optimized for the stretch growth behavior of that specific cell type. Additionally, further experiments on the limits of axonal stretch growth are needed to evaluate both our choice of growth evolution law and the robustness of our model predictions. Finally, we chose a phenomenological evolution law for the growth parameter that allows growth to accelerate over time. While the phenomenological model reproduces experimentally observed behavior, it does not provide a mechanistic explanation for the observed behavior. For example, the viscous relaxation time constant we used here is several orders of magnitude larger than the values reported for red blood cell and neuronal growth cone membranes, which are on the order of 10^{-1}s [7,21]. This could be because the experimental measurements were taken on the plasma membrane alone, whereas the viscosity in our model characterizes the behavior of the entire axon including the plasma membrane, cytosol, and cytoskeleton. A more mechanistic model of the axon, with all its subcellular structures and organelles, could provide additional details about the load transfer within the axon [11] and the biochemistry of axonal failure [13,15]. However, the modular nature of our model facilitates its implementation in finite element analyses of axon elongation devices or other studies of axonal growth.

In axonal stretching, growth occurs on the order of hours, but applied deformations occur on the order of seconds. Limitations on axonal stretch growth are found in both regimes. By including both viscoelasticity and growth in a model of stretch-mediated axonal growth, we were able to predict disconnection behavior at both time scales. While growth rate governs disconnection at long time scales, the viscoelastic constitutive behavior of the axon governs disconnection at short time scales. Accounting for both viscoelasticity and growth provides more insight into the phenomenon of stretch-mediated growth than the behavior at either time scale alone.

Acknowledgements This work was supported by the National Science Foundation Graduate Research Fellowship DGE 1656518 and the Stanford School of Engineering Fellowship to Lucy M. Wang and by the National Science Foundation Grant CMMI 1727268 and the Stanford Bio-X IIP seed Grant to Ellen Kuhl.

Compliance with ethical standards

Conflict of interest The authors declare that they have no conflict of interest.

References

1. Abe I, Ochiai N, Ichimura H, Tsujino A, Sun J, Hara Y (2004) Internodes can nearly double in length with gradual elongation of the adult rat sciatic nerve. J Orthop Res 22:571–577
2. Arnaoutoglou CM, Sakellariou A, Vekris M, Mitsionis GI, Korompilias A, Ioakim E, Harhantis A, Beris A (2006) Maximum intraoperative elongation of the rat sciatic nerve with tissue expander: functional neurophysiological, and histological assessment. Microsurgery 26:253–261
3. Bray D (1984) Axonal growth in response to experimentally applied mechanical tension. Dev Biol 102:379–389
4. Budday S, Sommer G, Holzapfel GA, Steinmann P, Kuhl E (2017) Viscoelastic parameter identification of human brain tissue. J Mech Beh Biomed Mat 74:463–476
5. Chada S, Lamoureux P, Buxbaum RE, Heidemann SR (1997) Cytomechanics of neurite outgrowth from chick brain neurons. J Cell Sci 110:1179–1186
6. Dagg AI, Foster JB (1982) The giraffe, its biology, behavior and ecology. Van Nostrand Reinhold, New York
7. Dai J, Sheetz MP (1995) Mechanical properties of neuronal growth cone membranes studied by tether formation with laser optical tweezers. Biophys J 68:988–996
8. Dai J, Sheetz MP, Wan X, Morris CE (1998) Membrane tension in swelling and shrinking molluscan neurons. J Neurosci 18:6681–6692
9. Dennerll TJ, Lamoureux P, Buxbaum RE, Heidemann SR (1989) The cytomechanics of axonal elongation and retraction. J Cell Biol 109:3073–3083
10. de Rooij R, Miller KE, Kuhl E (2017) Modeling molecular mechanisms in the axon. Comput Mech 59:523–537
11. de Rooij R, Kuhl E (2018) Microtubule polymerization and cross-link dynamics explain axonal stiffness and damage. Biophys J 114:201–212
12. de Rooij R, Kuhl E, Miller KE (2018) Modeling the axon as an active partner with the growth cone in axonal elongation. Biophys J 115:1783–1795
13. de Rooij R, Kuhl E (2018) Physical biology of axonal damage. Front Cell Neurosci 12:144
14. Evans E, Heinrich V, Ludwig F, Rawicz W (2003) Dynamic tension spectroscopy and strength of biomembranes. Biophys J 85:2342–2350
15. García JA, Pena JM, McHugh S, Jérusalem A (2012) A model of the spatially dependent mechanical properties of the axon during its growth. CMES Comp Mod Eng Sci 87:411–432
16. García-Grajales JA, Jérusalem A, Goriely A (2017) Continuum mechanical modeling of axonal growth. Comput Methods Appl Mech Eng 314:147–163
17. Goriely A, Budday S, Kuhl E (2015) Neuromechanics: from neurons to brain. Adv Appl Mech 48:79–139
18. Harrison RG (1935) On the origin and development of the nervous system studied by the methods of experimental embryology. Proc R Soc Lond B 118:155–196
19. Hategan A, Law R, Kahn S, Discher DE (2003) Adhesively-tensed cell membranes: lysis kinetics and atomic force microscopy probing. Biophys J 85:2746–2759
20. Hentz VR, Rosen JM, Xiao SJ, McGill KC, Abraham G (1993) The nerve gap dilemma: a comparison of nerves repaired end to end under tension with nerve grafts in a primate model. J Hand Surg Am 18:417–425
21. Hochmuth RM, Buxbaum KL, Evans EA (1980) Temperature dependence of the viscoelastic recovery of red cell membrane. Biophys J 29:177–182
22. Holland MA, Miller KE, Kuhl E (2015) Emerging brain morphologies from axonal elongation. Ann Biomed Eng 43:1640–1653
23. Howarth HM, Alaziz T, Nicolds B, O'Connor S, Shah SB (2019) Redistribution of nerve strain enables end-to-end repair under tension without inhibiting nerve regeneration. Neural Regen Res 14:1280–1288

24. Kolodkin AL, Tessier-Lavigne M (2011) Mechanisms and molecules of neuronal wiring: a primer. Cold Spring Harb Perspect Biol 3:a001727
25. Lowery LA, Van Vactor D (2009) The trip of the tip: understanding the growth cone machinery. Nat Rev Mol Cell Biol 10:332–343
26. Menzel A (2005) Modelling of anisotropic growth in biological tissues. Biomech Mod Mechanobio 3:147–171
27. Menzel A, Kuhl E (2012) Frontiers in growth and remodeling. Mech Res Commun 42:1–14
28. McDonald DS, Bell MS (2010) Peripheral nerve gap repair facilitated by a dynamic tension device. Can J Plast Surg 18:e17–e19
29. O'Toole M, Lamoureux P, Miller KE (2008) A physical model of axonal elongation: force, viscosity, and adhesions govern the mode of outgrowth. Biophys J 94:2610–2620
30. Pannese E (1994) Neurocytology: fine structure of neurons, nerve processes, and neuroglial cells. Thieme, Stuttgart
31. Pfister BJ, Iwata A, Meaney DF (2004) Extreme stretch growth of integrated axons. J Neurosci 24:7978–7983
32. Purohit PK, Smith DH (2016) A model for stretch growth of neurons. J Biomech 49:3934–3942
33. Simpson AHRW, Halliday J, Hamilton DF, Smith M, Mills K (2013) Limb lengthening and peripheral nerve function—factors associated with deterioration of conduction. Acta Orthop 84:579–584
34. Smith DH, Wolf JA, Meaney DF (2001) A new strategy to produce sustained growth of central nervous system axons: continuous mechanical tension. Tissue Eng 7:131–139
35. Sunderland IR, Brenner MJ, Singham J, Rickman SR, Hunter DA, Mackinnon SE (2004) Effect of tension on nerve regeneration in rat sciatic nerve transection model. Ann Plast Surg 53:382–387
36. Terzis J, Faibisoff B, Williams B (1975) The nerve gap: suture under tension vs. graft. Plast Reconstr Surg 56:166–170
37. Van Veen MP, Van Pelt J (1994) Neuritic growth rate described by modeling microtubule dynamics. Bull Math Biol 56:249–273
38. Vaz KM, Brown JM, Shah SB (2014) Peripheral nerve lengthening as a regenerative strategy. Neural Regen Res 9:1498–1501
39. Yousef MAA, Dionigi P, Marconi S, Calligaro A, Cornaglia AI, Alfonsi E, Auricchio F (2015) Successful reconstruction of nerve defects using distraction neurogenesis with a new experimental device. Basic Clin Neurosci 6:253–264
40. Zheng J, Lamoureux P, Santiago V, Dennerll T, Buxbaum RE, Heidemann SR (1991) Tensile regulation of axonal elongation and initiation. J Neurosci 11:1117–1125